Structural analysis of injection-moulded semicrystalline polymers by Fourier transform infra-red spectroscopy with photoacoustic detection and differential scanning calorimetry: 1. Poly(ethylene terephthalate)

L. Quintanilla, J. C. Rodríguez-Cabello, T. Jawhari and J. M. Pastor*
Dept Física de la Materia Condensada, Facultad de Ciencias, Escuela Técnica Superior de Ingenieros Industriales (ETSII), Universidad de Valladolid, 47011 Valladolid, Spain
(Received 16 December 1992; revised 10 February 1993)

Fourier transform infra-red spectroscopy coupled with photoacoustic detection (PA *FT*i.r.) has proved to be a useful tool for finding out about quantitative structural changes in solid materials. Poly(ethylene terephthalate) (PET) is a well known semicrystalline polymer that shows important changes on annealing. In order to obtain a complete picture of isomer distributions in industrial PET samples, spectroscopic measurements were correlated with differential scanning calorimetry (d.s.c.). The results obtained indicate that the structural characteristics of the thermally treated samples are related to the fabrication process. Two different strata in the plates can be distinguished: a skin layer and the core. The correlation between the apparent degree of crystallinity of the surface obtained by d.s.c. and the percentage of *trans* isomer obtained by PA *FT*i.r. allows the latter parameter to be separated into crystalline and amorphous *trans* isomer and to follow its evolution with the annealing process. Amorphous *trans* isomer vanishes at the primary isomerization ($\sim 100°C$) while crystalline *trans* and *gauche* conformations show sigmoidal evolution. At higher annealing temperatures ($> 140°C$) the ordered *trans* conformation shows an approximately linear increase at the expense of the *gauche* conformation. Finally, a direct correlation between the ordered *trans* isomer and the apparent degree of surface crystallinity can be made.

(Keywords: PA *FT*i.r.; d.s.c.; PET; isomerization; crystallinity)

INTRODUCTION

Poly(ethylene terephthalate) (PET) is a well known semicrystalline polymer with important applications and, therefore, is of high commercial interest. This material is widely used as films or fibres and, recently, as a reinforced compound to produce composite materials.

This paper focuses on the structural characterization of commercial injection-moulded semicrystalline PET. The detailed structural study of the matrix reinforced with glass fibre will be the subject of subsequent papers.

Sample preparation is often the most time-consuming part of spectroscopic analysis, including infra-red (i.r.) analysis. Diffuse reflectance has been proposed as a practical 'no preparation' i.r. technique. However, it works well only on highly scattering samples. Moreover, symmetrically shaped absorption bands are represented by asymmetric 'differential-like' band shapes[1,2]. On the other hand, the attenuated total reflection technique shows a great deal of uncertainty about contact between the sample and the high index crystal.

In the late 1970s, the feasibility of using photoacoustic Fourier transform infra-red (PA *FT*i.r.) spectroscopy as an analytical technique was demonstrated in studies of condensed phase samples when photoacoustic (PA) detection was combined with an interferometer and a large capacity data system[3]. The high throughput and multiplex advantages of the *FT*i.r. spectrometer have currently made PA *FT*i.r. a routine analytical technique with a desirable signal-to-noise ratio[4].

The general theory for the PA effect in condensed media was formulated in 1976 by Rosencwaig and Gersho[5], now commonly referred to as the RG theory. Some of the experimental advantages of this technique include[6,7]: since absorption of electromagnetic radiation is required before the PA signal can be generated, light that is transmitted or elastically scattered by the sample is not detected and hence does not interfere with the inherently absorptive PA spectroscopic measurements (PA spectra like absorption spectra in transmission); minimum sample preparation is necessary and any structural change due to the preparation process is avoided.

In spite of the uncontested importance of vibrational spectroscopy for the characterization of macromolecular structure, however, it should be emphasized that only a limited number of problems may be solved by its exclusive application. In the majority of cases, the maximum amount of structural information can be obtained

* To whom correspondence should be addressed

0032-3861/93/183787-09

only by an appropriate choice and combination of chemical and physical methods. Differential scanning calorimetry (d.s.c.) measurements have been performed as a complementary technique to the structural analysis of PET samples.

EXPERIMENTAL

Materials

The sample used was supplied by SNPE (France) as a 3 mm thick plate obtained by injection moulding of commercial PET (tradename PET 92T; *o*-chlorophenol viscosity ≈ 100; $M_w = 47\,000$; $M_n \approx 24\,000$). The PET was injected into the mould at a temperature of 260°C and at a pressure of 10 MPa. The temperature of the mould was fixed at 40°C and the injected sample was maintained in it for 10 s at a pressure of 95×10^5 Pa.

Samples ($3 \times 2 \times 3$ mm) were cut from the plates and introduced into an oven stabilized at annealing temperatures (T_{ann}) ranging from 65 to 230°C, kept there for 1 h and then cooled to room temperature.

PA FTi.r. measurements

PA *FT*i.r. spectra of PET samples were obtained at room temperature on a Mattson Cygnus 100 *FT*i.r. spectrometer equipped with a MTEC 200 PA cell. Two different sets of spectra were obtained: the first at 8 cm^{-1} resolution and averaged over 312 scans; the second at 4 cm^{-1} resolution and averaged over 1120 scans. The best signal-to-noise ratio was obtained with a mirror speed of 0.12 cm s^{-1}. Powdered carbon was used as a photoacoustically saturated (black) reference material.

D.s.c. measurements

The thermal analysis was carried out in an air atmosphere with specimens weighing in the range of 7–10 mg; the calibration of both temperature and melting enthalpy was made with a standard sample of indium.

The d.s.c. experiments were performed on Mettler TA4000 (DSC 30) equipment at a heating rate of 10°C min^{-1}; each thermogram was recorded from 25 to 320°C.

From the measured heat of fusion (ΔH_{exp}) an apparent degree of crystallinity ($\%C_{d.s.c.}$) was determined according to the equation:

$$\%C_{d.s.c.} = \frac{\Delta H_{exp}}{\Delta H^0} \quad (1)$$

where ΔH^0 is the heat of fusion of an ideal PET crystal. A value of 28.1 cal g^{-1} (117.7 J g^{-1}), as given by Mehta *et al.*[8], was used.

RESULTS AND DISCUSSION

Vibrational analysis

Vibrational spectra of PET have been studied in detail in a large number of papers[9–23]. In the crystalline state, PET is present in almost planar form according to X-ray diffraction analysis, where the ethylene glycol fragment has a *trans* structure. In the amorphous state, PET has a more complicated conformational composition and both *trans* and *gauche* conformations of the above segment can be present[9,10].

Thermal treatments in PET cause a clear change in the crystallinity of this material and consequently in the vibrational behaviour. These variations, although related to the crystallinity, are explained as being due to conformational changes. These changes have generally been attributed to either rotational isomerism in the ethylene glycol segments of the molecules or variations in the symmetry and resonance characteristics of the substituted benzenoid structure[11].

Photoacoustic characterization of the samples. The PA signal depends on geometric, optical and thermal parameters of the sample and, therefore, different spectroscopic information can be obtained in relation to the values of these parameters[5].

The geometric parameter is given by the thickness of the sample ($l = 3$ mm).

To calculate the optical parameters, it must be taken into account that the optical absorption coefficient (β) depends on the wavenumber of the radiation. In the experiments, quantitative measurements were only carried out over a frequency range[12] varying from 750 to 1000 cm^{-1}. Thus, β was calculated from the transmission *FT*i.r. spectrum for an unannealed PET film at the most characteristic bands, i.e. at 793, 845, 876, 898 and 973 cm^{-1}, which gives β values that range from 80 to 220 cm^{-1}. As a result, the optical absorption length, $l_\beta = \beta^{-1}$, ranges from 45 to 125 μm at these wavenumbers.

Finally, the thermal parameters were calculated from the thermal diffusivity value of PET[24] ($\alpha = K/C\rho = 14 \times 10^{-4}$ cm^2 s^{-1}), where K is the thermal conductivity, ρ is the density and C is the specific heat. According to the PA theory[5,7], the thermal diffusion length (μ) is given by:

$$\mu = \left(\frac{2\alpha}{w}\right)^{1/2} \quad (2)$$

where w is the angular modulation frequency that can be calculated from the modulation frequency, f:

$$w = 2\pi f \quad \text{and} \quad f = v\nu \quad (3)$$

where v is the optical velocity of the interferometer and ν is the wavenumber of the i.r. radiation. In the Michelson design interferometer used in these experiments, v is two times greater than the mirror velocity.

Using the above data for PET:

$$\mu = \frac{430}{\nu^{1/2}} \quad (4)$$

In the experiments reported here, the spectral range was 750–1000 cm^{-1} and, consequently, the above expression at the band positions ranges from 14 to 15 μm.

Therefore, $l \gg \beta^{-1}$ and $\mu < \beta^{-1}$; thus, the material to be analysed can be considered as an optically opaque and thermally thick solid. According to RG theory, in this case only the light absorbed within the thermal diffusion length contributes to the PA signal. Therefore, the structural information presented below is characteristic of a surface depth of ~ 15 μm.

Vibrational spectra. PA *FT*i.r. spectra of unannealed and annealed PET at 90, 150 and 205°C are shown in *Figure 1*. The absorbance for the bands at 1470, 1337, 973 and 845 cm^{-1} increases in intensity during annealing, while that of those near 1453, 1370, 1040 and 898 cm^{-1} decreases. The first group of bands was found to be associated with the *trans* conformation of the ethylene

glycol segments and the second with the *gauche* ones. The remaining i.r. bands, those at 1580, 1504, 1410 and 876 cm^{-1}, have been assigned to ring modes[11]. Finally, the 793 cm^{-1} band was reported as an internal reference band[12] and will be used as our reference band.

The bands situated at about 1730, 1275 and 1125 cm^{-1} show a strikingly different shape with regard to the other bands. They include very wide spectral ranges (hundreds of wavenumbers) and do not have a well defined maximum, but rather a wide plateau. In these spectral regions, PET shows a large optical absorption coefficient. Therefore, the relationship between the PA parameters has been changed and is now, $\mu > \beta^{-1}$ with $l \gg \beta^{-1}$; thus, the solid is optically opaque and thermally thin, according to the RG theory. That is, there is PA 'opaqueness' as well as optical opaqueness, since the PA signal is independent of β. In this particular situation, no structural information can be obtained from these bands.

Quantitative analysis. As it has already been reported[11,12], the above spectral changes were caused by conformational changes and the best bands to monitor them quantitatively are the bands at 973 cm^{-1} ($O-CH_2$, stretching) and 898 cm^{-1} (CH_2, rocking)[11,13] (*Figure 2*).

In i.r. spectroscopy, peak heights are often used for quantitative analysis. Peak heights were measured with respect to baselines drawn between the valleys on either side. For a certain pair of peaks which overlap (876 and 898 cm^{-1}), the baseline was chosen to include both peaks.

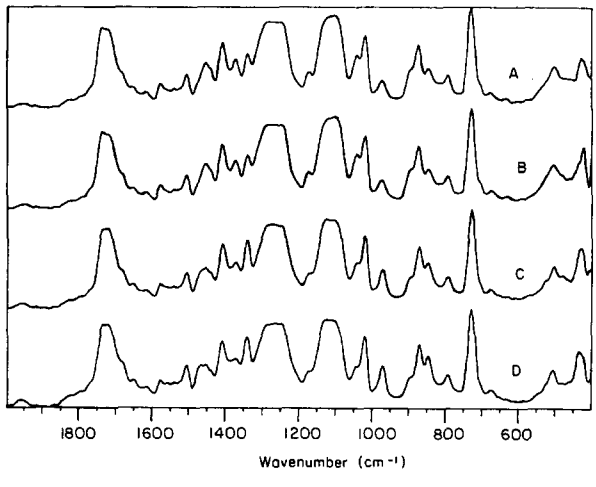

Figure 1 PA *FT*i.r. spectra of unannealed PET (A) and annealed at 90°C (B), 150°C (C) and 205°C (D) in the spectral range 400–2000 cm^{-1} (8 cm^{-1} resolution)

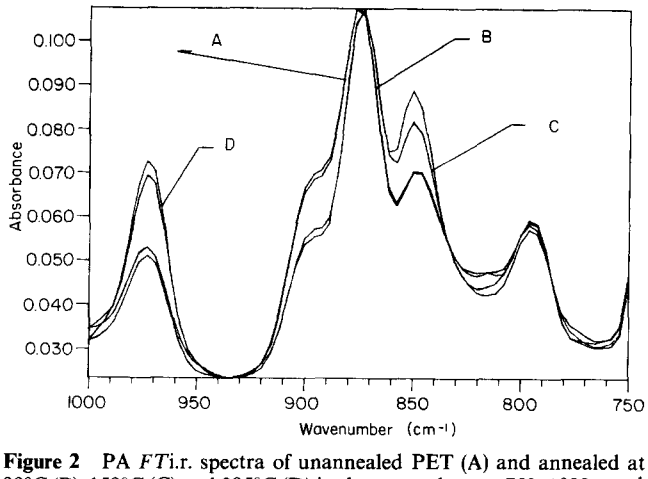

Figure 2 PA *FT*i.r. spectra of unannealed PET (A) and annealed at 90°C (B), 150°C (C) and 205°C (D) in the spectral range 750–1000 cm^{-1} (8 cm^{-1} resolution)

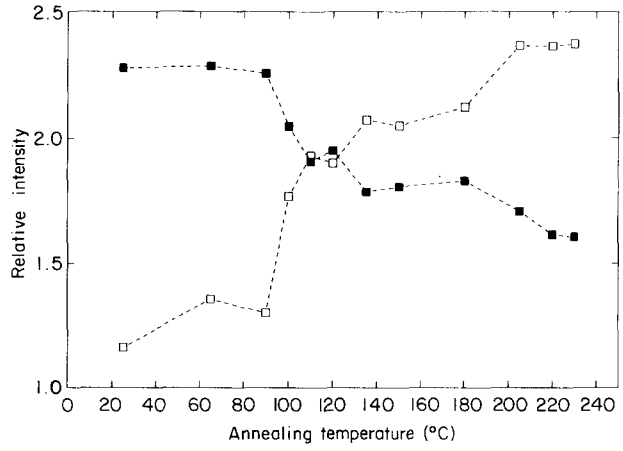

Figure 3 Relative intensities of the band at 973 cm^{-1} (□) and 898 cm^{-1} (■) *versus* annealing temperature

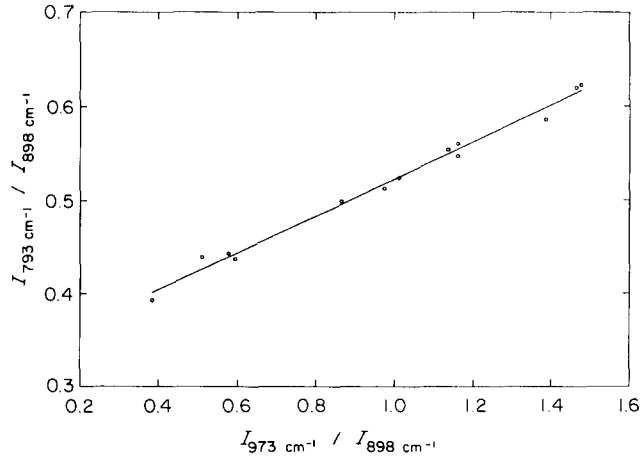

Figure 4 Verification of the two-phase conformational model in PET: $I_{793\,cm^{-1}}/I_{898\,cm^{-1}}$ *versus* $I_{973\,cm^{-1}}/I_{898\,cm^{-1}}$

Deconvolution and subtraction studies have demonstrated that the 973 cm^{-1} band can be separated into two components; one at 975 cm^{-1} which is associated with an amorphous *trans* component and the other at 973 cm^{-1} which is involved with the ordered zone[14–16]. Thus, the 973 cm^{-1} band provides information on the ordered and amorphous phases, corresponding to the ethylene glycol fragment.

The intensity ratios I_{973}/I_{793} and I_{898}/I_{793} *versus* annealing temperature are plotted in *Figure 3*.

Although PET is a semicrystalline polymer, spectra of the *trans* isomer in the crystalline and disordered phases must be sufficiently similar so as not to be resolved under these experimental conditions[12]. According to this last observation, PET would satisfy a two-phase conformational model, i.e.:

$$1 = p_1 \frac{I_{973}}{I_{793}} + p_2 \frac{I_{898}}{I_{793}} \tag{5}$$

where p_1 and p_2 are the 973 and 898 cm^{-1} band weights related to the interaction of radiation matter.

From this equation, we obtain:

$$\frac{I_{793}}{I_{898}} = p_1 \frac{I_{973}}{I_{898}} + p_2 \tag{6}$$

and the representation of this equation is shown in *Figure 4* with a very good fitting. The least-squares curve fitting technique was carried out in order to obtain the p_1 and p_2 parameters. The values

$$p_1 \frac{I_{973}}{I_{793}} \quad \text{and} \quad p_2 \frac{I_{898}}{I_{793}}$$

represent the individual isomer distributions at different annealing temperatures (*Figure 5a*). The evaluation of the addition of both isomers allows the experimental error to be estimated at ~4–5% (*Figure 5b*).

In *Figure 5a* only the evolution of total *trans* and *gauche* isomers with T_{ann} can be analysed. However, our main purpose is to split up the curve of total *trans* into its two components, the *trans* conformers involved in the amorphous and in the crystalline regions, and to follow its dependence on the thermal treatment. This problem will be solved later when combining these results with another independent technique such as d.s.c.

It can be noted that *Figures 3* and *5a* show the well known two-stage structural reorganization process that usually takes place in PET with thermal treatment[12,18,19]. Below the glass transition ($T_g \approx 75$–80°C), there is little change in the isomer distributions with T_{ann}. When this temperature is exceeded, there is a drastic change in the relative amounts of *gauche* and *trans* isomers (sigmoidal curve).

At higher T_{ann} (>140°C), there is a second change in the slope of the *gauche* and *trans* isomers *versus* T_{ann}.

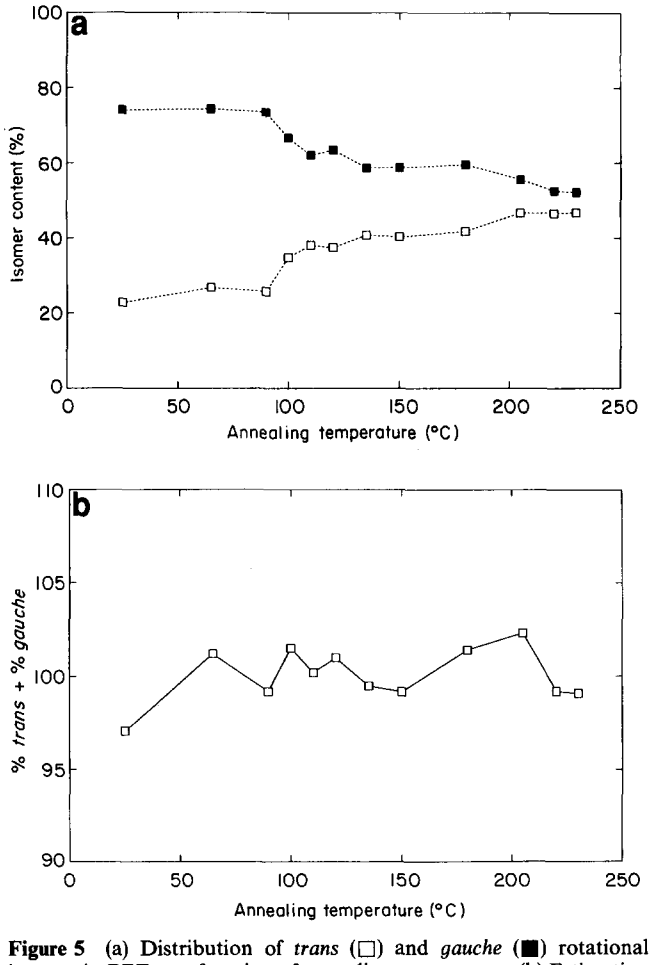

Figure 5 (a) Distribution of *trans* (□) and *gauche* (■) rotational isomers in PET as a function of annealing temperature. (b) Estimation of spectroscopic experimental error: (*%trans*+*%gauche*) *versus* annealing temperature

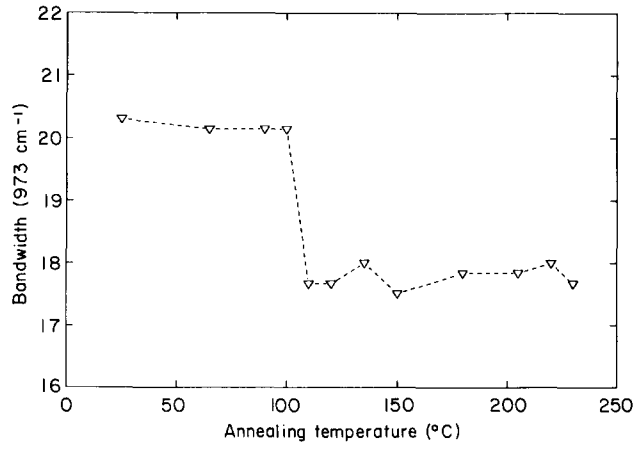

Figure 6 Bandwidth of the 973 cm^{-1} band *versus* annealing temperature

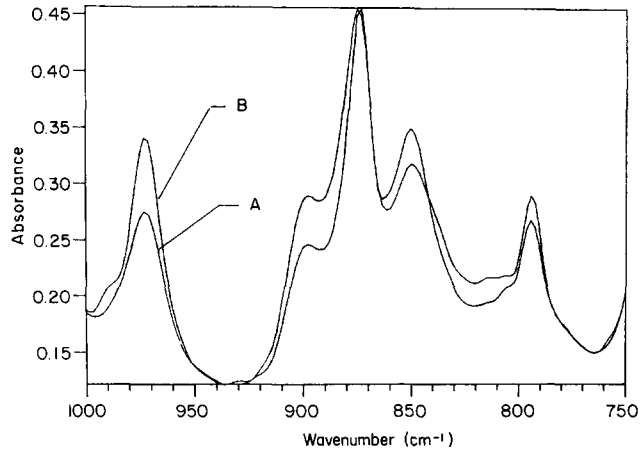

Figure 7 PA *FT*i.r. spectra of unannealed PET (A) and annealed at 205°C (B) in the spectral range 750–1000 cm^{-1} (4 cm^{-1} resolution)

The mobility of the segments is high enough to permit segmental rearrangements, so more crystallization occurs.

The bandwidth of the band at 973 cm^{-1} shows a sharp decrease when T_{ann} reaches the primary transition (*Figure 6*). Since contributions of ordered and disordered *trans* isomers can be found in this band, it can be considered that the ratio between the ordered (narrow) and disordered (broad) components was changed by the decrease of the disordered component[17].

Analysis of benzene ring vibration modes. No variation in the intensity and frequency of the 1580, 1504 and 1410 cm^{-1} bands could be detected. However, the situation is quite different with regard to the 876 cm^{-1} band (*Figures 2* and *7*) which is assigned to the out-of-plane C–H benzene ring deformation vibration[17]. It must be pointed out that the frequency shift from 876 to 873 cm^{-1} experimentally observed when T_{ann} is >90°C is in good agreement with other work[21]. Similar changes were observed by Hutchinson and Ward on uniaxially stretched films of PET[22]. From i.r. dichroism measurements[17], it follows that this vibration is nearly perpendicular to the molecular axis. It is supposed that this vibrational mode, perpendicular to the benzene ring, is extremely sensitive to the presence of other benzene rings. The primary isomerization involves rotation

of the ethylene glycol fragments of the polymer chains as well as the corresponding changes in symmetry of benzenoid segments to obtain the closest packing in crystalline regions[21]. Thus, the above frequency shift is directly related to the packing change due to primary transformation.

Chain folding band. A small band at $\sim 988\,cm^{-1}$ was detected when high spectral resolution was used (*Figure 7*). This shoulder near the $973\,cm^{-1}$ band was reported to be associated with chain folding[20,23]. This phenomenon arises from the fact that the highest annealing treatments are supposed to remove crystal imperfections and to improve chain packing at the amorphous–crystalline interphase.

Thermal analysis

The melting behaviour of annealed semicrystalline PET has been studied over the last 25 years; however, this has led to contradictory interpretations[25–30].

It is interesting to consider the d.s.c. thermograms in *Figure 8*. The glass transition, an exothermic and two endothermic peaks that depend on the thermal history, can be observed.

For unannealed samples, the glass transition is found at 77°C. The exothermic peak near 128°C indicates that further crystallization takes place during the heating run in the d.s.c. pan; the endothermic peak at ~258°C indicates the melting of PET.

Substantial changes occur in the thermogram of the samples that had undergone previous annealing. The glass transition peak appears as strong as that of the unannealed sample for T_{ann} below 100–110°C. It is also observed that the intensity of the exothermic crystallization peak decreases and, eventually, shifts downward with increasing T_{ann}.

For samples annealed at higher temperature than that of the primary transition temperature, this second-order transition becomes barely perceptible.

These d.s.c. results are in excellent agreement with the previous spectroscopic data where the clear variation at $T_{ann} \approx 100$–110°C corresponds to the primary transformation process (sigmoidal curve). PET samples undergo a solid-state (or 'cold') exothermic crystallization during heating in the d.s.c. experiment[28]. The untreated PET sample shows the highest degree of latent heat of crystallization during scanning; when T_{ann} rises, the exothermic peak decreases and, finally, vanishes at $T_{ann} \approx 110$°C. Experimental data related to the exothermic and endothermic peaks are shown in *Table 1*.

An endothermic low melting peak (LM peak) appears in the d.s.c. thermograms of samples annealed longer than the primary transformation stage followed by another endothermic high melting peak (HM peak)[28].

A number of proposals have been made on the origin of the multiple fusion endotherms in PET. Despite conflicting views, there is a growing trend favouring the interpretation of the melting of crystals formed during the heating experiment by a partial melting and recrystallization mechanism[28].

Annealing treatment of PET at low temperatures produces small crystallites with a low degree of perfection. During the d.s.c. scan some of these crystals melt and recrystallize with a higher perfection[25,27–30]. This explanation does not necessarily imply that the crystallites melt completely, there may exist some type of internal reorganization process which leads to a higher perfection[25].

Table 1 Thermal parameters of the unannealed sample and annealed up to the primary isomerization temperature[a]

T_{ann} (°C)	ΔH_{crys} ($J\,g^{-1}$)	T_{crys} (°C)	ΔH_f ($J\,g^{-1}$)	T_f (°C)	ΔH_{net} ($J\,g^{-1}$)
Unannealed	11.6	128	46	258	34
65	10.3	128	46	258	36
90	9.9	128	44	260	34
100	5.7	125	48	259	42
110	–	–	47	259	47
120	–	–	47	262	47

[a] ΔH_{crys}, latent heat of crystallization; T_{crys}, crystallization temperature; ΔH_f, heat of fusion; T_f, melting temperature

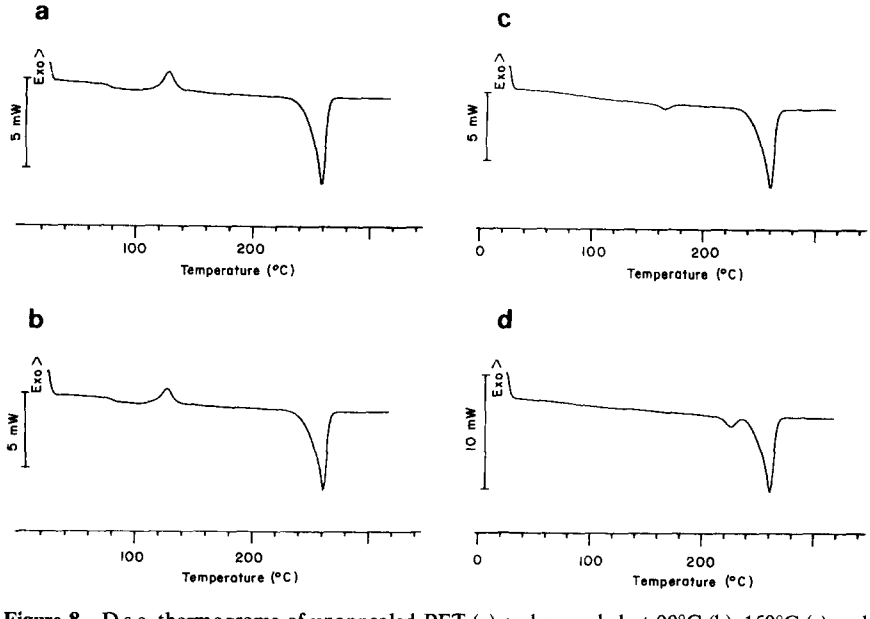

Figure 8 D.s.c. thermograms of unannealed PET (a) and annealed at 90°C (b), 150°C (c) and 205°C (d)

Characteristic parameters related to both the LM and HM peaks are presented in *Table 2*. The LM peak constantly shifts toward higher temperatures and grows in size with increasing T_{ann} and, eventually, becomes comparable in size with the HM peak. Since the HM peak temperature remains almost constant over a large range of T_{ann}, the melting temperature of the LM peak (T_m) can be used to study the effect of annealing. The LM peak shift may indicate that the original crystalline structure transforms to a more stable one due to the annealing process.

A plot of the two melting temperatures *versus* T_{ann} is given in *Figure 9*. It can be observed that T_m increases linearly at ~15–20°C above T_{ann}. This endothermic peak can be attributed to crystal thickening as well as to crystal perfection and fold-surface smoothing of the crystalline layers. With our results, we found the relation:

$$T_m = 13 + 1.02T_{ann} \quad (7)$$

Table 2 also shows that the integrated area of the first peak (ΔH_{LM}) increases with T_{ann} at the expense of the second peak (ΔH_{HM}), but only small changes of the overall heat of fusion ($\Delta H = \Delta H_{LM} + \Delta H_{HM}$) are observed. The apparent d.s.c. trace between the LM and HM peaks varies with thermal history in the secondary transformation stage. Thus, the net area between this trace and the constructed baseline from the beginning of the LM peak to the end of the HM peak[28] (ΔH_{net}) is always found to be higher than ΔH.

In order to obtain the evolution of the heat of fusion with the thermal treatment, we shall assume that the values required for the fusion and crystallization are the same, but with opposite sign, at least, for d.s.c. with slow heating rates[31]. Considering endothermic and exothermic peaks, the net heat of fusion is, therefore, $\Delta H_{net} = \Delta H_f - \Delta H_{crys}$ (see *Tables 1* and *2*).

Table 2 Thermal parameters of the annealed samples beyond the primary isomerization temperature

T_{ann} (°C)	ΔH_{LM} (J g^{-1})	ΔH_{HM} (J g^{-1})	$\Delta H_{LM} + \Delta H_{HM}$ (J g^{-1})	ΔH_{net} (J g^{-1})
135	2.2	46.4	48.6	51
150	2.8	45.5	48.3	51
180	3.5	43.0	46.5	50
205	4.4	42.3	46.7	52
220	–	–	–	55
230	–	–	–	57

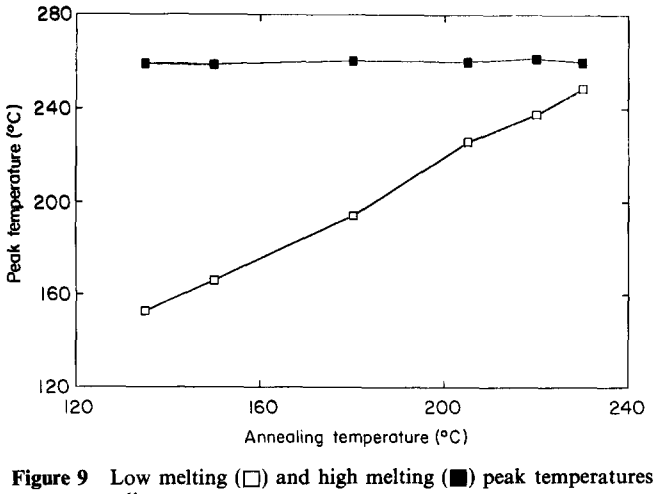

Figure 9 Low melting (□) and high melting (■) peak temperatures *versus* annealing temperature

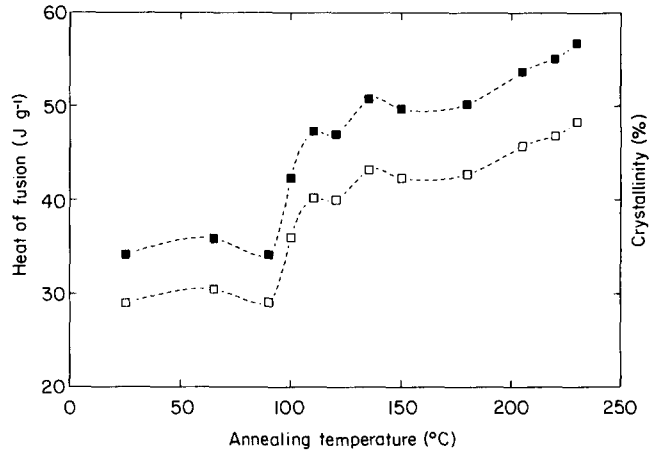

Figure 10 Net heat of fusion (■) and crystallinity (□) *versus* annealing temperature

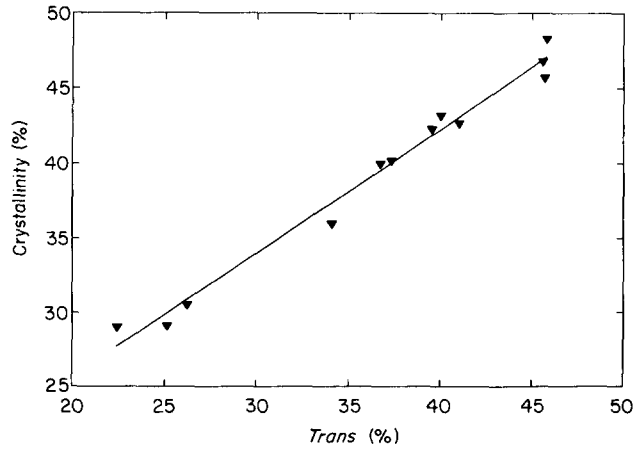

Figure 11 D.s.c. crystallinity (bulk) *versus trans* isomer content

The net heat of fusion and percentage crystallinity are plotted in *Figure 10*. Both show the sigmoidal curve and the linear slope at the highest T_{ann}, in good agreement with results previously obtained by PA *FT*i.r.

Quantitative correlations between PA FTi.r. *and d.s.c. measurements*

The main purpose of this work is the analysis of the total conformational structure of PET samples and its dependence on T_{ann}. This can be carried out by correlating the results obtained previously by spectroscopic and calorimetric methods.

In *Figure 11*, the percentage of crystallinity *versus* the *trans* isomer content obtained by PA *FT*i.r. is plotted. The least-squares curve fitting method gives the following straight line:

$$\%C_{d.s.c.} = 9.2 + 0.83\ (\%trans) \quad (8)$$

The d.s.c. technique measures the amount of heat required to melt the crystalline regions of the sample; i.r. spectroscopy measures the concentration of total *trans* isomer. Therefore, 'crystallinity' values based on the intensity of i.r. bands must be higher than d.s.c. crystallinity values because d.s.c. does not measure the contributions of isolated ordered chains to short-range

order[32], which may contribute to i.r. measurements. However, the positive intercept on the ordinate axis of the above expression implies the opposite behaviour and, consequently, further consideration must be given to the problem.

The PA signal provides information on an effective thickness of the sample at $\sim 15\,\mu m$ from the sample surface whereas the d.s.c. values obtained were mainly characteristic of the bulk.

Another aspect that has to be considered is the influence of the fabrication process on the samples. Injection moulding involves two factors which are of great importance[33,34]: (1) mould walls operate as a nucleant agent and the layers in contact with the mould are the most highly shear-stressed, whereas in the bulk the molecules are less oriented; (2) as the material becomes in contact with the cold mould, a rapid cooling occurs whereas in the bulk the molecules can crystallize better. As a result, the degree of crystallization should be higher in the core than the surface and, at least, two strata can be imagined: a thin skin layer mainly 'amorphous' and a 'crystalline' core[35]. To verify this assumption, we cut films of the sample surface and, again, d.s.c. runs were carried out under the same experimental conditions as those described above.

In *Figure 12a*, endothermic melting peaks of unannealed bulk sample (solid line) and surface sample (broken line) are shown. Two main differences were detected: first, the halfwidth of the first peak (bulk) is less than that of the second (surface) and, consequently, a more homogeneous size crystal distribution is observed in the bulk; secondly, the position of the melting peak of bulk sample is at 257.7°C and at 256.6°C for the surface. Thus, near the mould surface the crystals form and grow in a more irregular way than in the bulk.

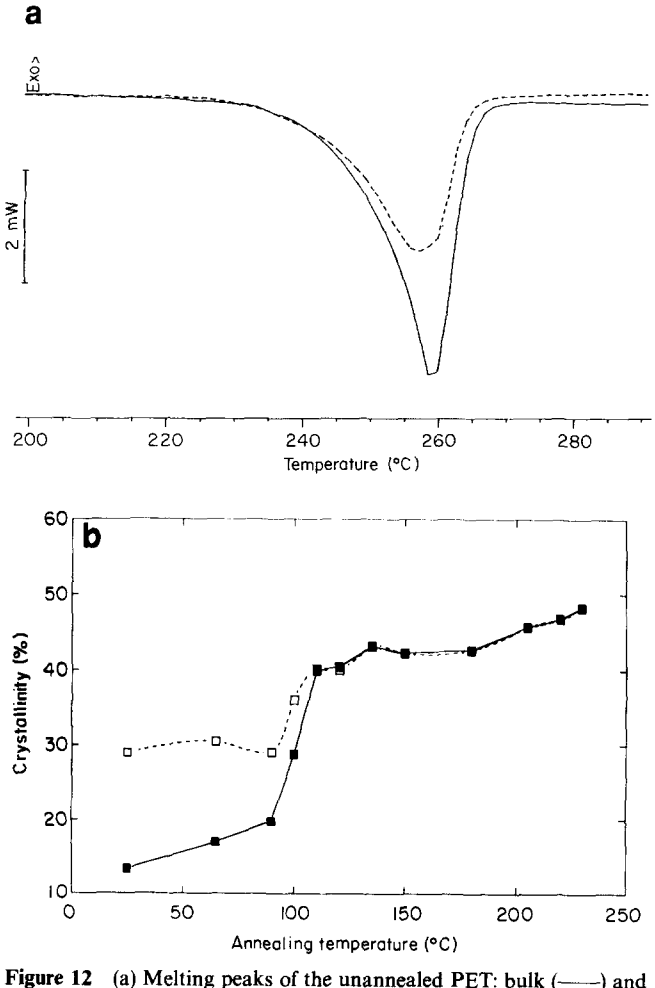

Figure 12 (a) Melting peaks of the unannealed PET: bulk (——) and surface (– – –). (b) Evolution of surface (■) and bulk (□) crystallinity (obtained by d.s.c.) with annealing temperature

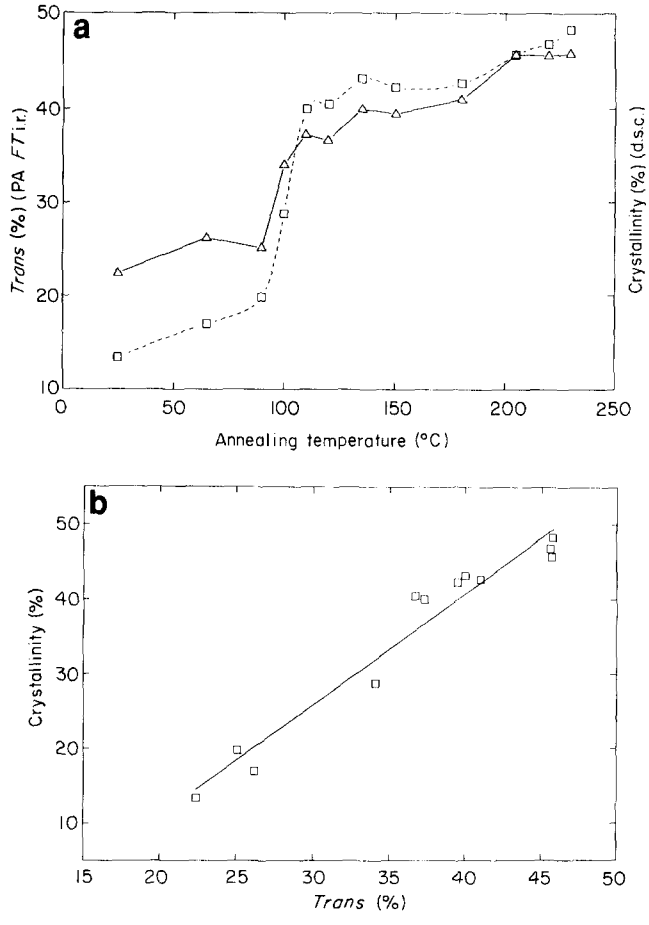

Figure 13 (a) Evolution of *trans* isomer content obtained by PA *FT*i.r. (△) and surface crystallinity obtained by d.s.c. (□) with annealing temperature. (b) Correlation between surface crystallinity and *trans* isomer content

Both bulk and surface crystallinity evolution are shown in *Figure 12b*. Below $T_{ann} \approx 110°C$, an important difference ($\sim 15\%$) between both curves can be detected. When the thermal treatment rises, the difference disappears and the plots overlap because the sample becomes homogeneous and the different layers cannot be distinguished.

It can be observed in *Figure 13a* that the total *trans* isomer content obtained by PA *FT*i.r. is higher than the degree of surface crystallinity obtained by d.s.c. at low T_{ann}; however, both are quite similar at high T_{ann}.

The surface crystallinity value by d.s.c. *versus* the *trans* isomer content by PA *FT*i.r. is plotted in *Figure 13b* and the least-square curve fitting method gives the straight line:

$$\%C_{d.s.c.} = 1.5\ (\%trans) - 18.8 \qquad (9)$$

This expression can be written as:

$$\%C_{d.s.c.} = m_{exp}(t_c + t_a) + ord_{exp} \qquad (10)$$

where t_c and t_a are the crystalline and amorphous *trans* isomer contents and m_{exp} and ord_{exp} are the slope and the intercept on the ordinate axis of the 'experimental' straight line.

Assuming that the latent heat of fusion is only due to the melting of crystalline *trans* isomers, we can write the 'ideal' crystallinity as:

$$\%C_{d.s.c.} = t_c \quad (11)$$

Identifying (10) and (11), we obtain with our experimental data:

$$t_a = 13 - 0.33\ \%C_{d.s.c.} \quad (12)$$

For a glassy amorphous sample ($\%C_{d.s.c.} = 0$) an extrapolated *%trans* value of 13% can be found. This value agrees with other authors proposing from 10 ± 3 to 14%[12,16,22,36]. Studies relate this amorphous *trans* conformation with some kind of order in the amorphous regions in PET[36,37].

Using this method a complete picture of the individual isomer distribution for every T_{ann} can be obtained. The percentage of each isomer is plotted in *Figure 14 versus* T_{ann}. The content of amorphous *trans* isomer decreases quickly and vanishes once T_{ann} overcomes primary isomerization.

In this figure, ordered *trans* and *gauche* isomers show a sigmoidal evolution and only at the highest T_{ann} is there an approximately linear increase of crystalline *trans* at the expense of the *gauche* conformation (secondary isomerization) with T_{ann} given by the relation:

$$t_c = 26 + 9 \times 10^{-2} T_{ann} \quad (13)$$

Finally, in *Figure 15* the crystalline *trans* isomer (t_c) and the surface crystallinity by d.s.c. for different T_{ann} values were correlated (diagonal corresponds to complete correlation). A good agreement between both representations is observed.

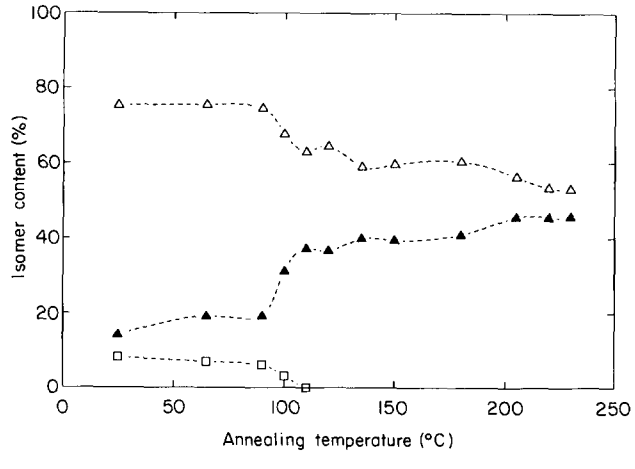

Figure 14 Distribution of rotational isomers in injection-moulded semicrystalline PET as a function of annealing temperature: *gauche* (△); crystalline *trans* (▲); amorphous *trans* (□)

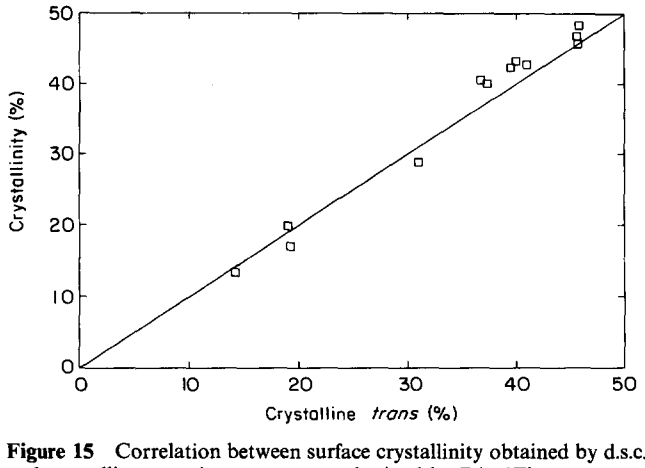

Figure 15 Correlation between surface crystallinity obtained by d.s.c. and crystalline *trans* isomer content obtained by PA *FT*i.r.

CONCLUSIONS

The study carried out shows that PA *FT*i.r. can be used as a method to prove quantitative structural microstructure changes in PET. First, the PA characterization of PET samples was performed in order to know what information is provided by the PA *FT*i.r. technique; in this particular case, structural information can be obtained in the spectral area of 750–1000 cm^{-1}. However, PA *FT*i.r. introduces some distortions in the spectral regions that are PA saturated, where no information about the structural characteristics of the sample can be obtained.

Making use exclusively of i.r. data and analysing the bands at 973 cm^{-1} (*trans*), 898 cm^{-1} (*gauche*) and 793 cm^{-1} (reference), it was demonstrated that PET satisfies a two-phase conformational model. Spectroscopic behaviour of injection-moulded PET is similar to that for annealed amorphous films and the primary and secondary isomerizations were monitored by the conformational changes in *trans* and *gauche* isomer contents: the sigmoidal curve (primary transformation) at low T_{ann} values and a linear evolution at the highest values (secondary isomerization).

Besides the intensity changes in the bands related to ethylene glycol segments, the effects of primary transformation can be followed through frequency shift (876 cm^{-1} band) and decreasing bandwidth (973 cm^{-1} band).

The thermal behaviour of commercial samples agrees well with that of annealed amorphous films. The glass transition and the exothermic peak of induced crystallization due to d.s.c. heating tend to disappear when the T_{ann} overcomes the primary isomerization. In the range of secondary isomerization, the LM and HM peaks were obtained and the relationship between the LM peak and the previous thermal process was monitored. From the integrated area of the secondary transformation range, the d.s.c. crystallinity value *versus* T_{ann} was obtained and shows a similar evolution to that of *trans* isomer content *versus* T_{ann}. Thus, a quantitative correlation can be made.

The influence of the fabrication process becomes very important to the analysis. At least two strata in plates of injection-moulded semicrystalline PET can be noted: a thin skin mainly 'amorphous' and a 'crystalline' core.

Based on the correlation of PA *FT*i.r. and d.s.c. surface measurements, the total *trans* isomer content could be separated into amorphous and crystalline components. The first tends to vanish at the primary isomerization while crystalline *trans* and *gauche* conformations show sigmoidal evolution. At the highest T_{ann} values, ordered *trans* shows a linear increase. This behaviour agrees well with previous observations on annealed amorphous films. Finally, a direct relationship between ordered *trans* and the apparent degree of surface crystallinity calculated by d.s.c. can be made.

ACKNOWLEDGEMENTS

The authors wish to thank the Comision Interministerial de Ciencia y Tecnología (Program MAT90-914) and Junta de Castilla y León (1605/90) for financial support.

REFERENCES

1 Fuller, M. P. and Griffiths, P. R. *Anal. Chem.* 1978, **50**, 1906
2 Fuller, M. P. and Griffiths, P. R. *Am. Lab.* 1978, **10** (10), 69
3 Rockley, M. G. *Chem. Phys. Lett.* 1979, **68**, 455
4 Graham, T. A., Grim III, W. M. and Fateley, W. G. 'Fourier Transform Infrared Photoacoustic Spectroscopy of Condensed-Phase Samples', Vol. 4, Academic Press, London, 1985, p. 345
5 Rosencwaig, A. and Gersho, A. *J. Appl. Phys.* 1976, **47**, 64
6 Vidrine, D. W. *Appl. Spectrosc.* 1980, **34**, 314
7 Rosencwaig, A. 'Photoacoustics and Photoacoustic Spectroscopy', Wiley, New York, 1980, p. 4
8 Mehta, A., Gaur, U. and Wunderlich, B. *J. Polym. Sci., Polym. Phys. Edn* 1978, **16**, 289
9 Ward, I. M. and Wilding, M. A. *Polymer* 1977, **18**, 327
10 Miyake, A. *J. Polym. Sci.* 1959, **38**, 479
11 Boerio, F. J. and Bahl, S. K. *J. Polym. Sci., Polym. Phys. Edn* 1976, **14**, 1029
12 Lin, S. B. and Köenig, J. L. *J. Polym. Sci., Polym. Phys. Edn* 1983, **21**, 2277
13 Sheiko, S. S., Vainilovitch, I. S. and Magonov, S. N. *Polym. Bull.* 1991, **25**, 499
14 Yazdanian, M., Ward, I. M. and Brody, H. *Polymer* 1985, **26**, 1779
15 d'Esposito, L. and Köenig, J. L. *J. Polym. Sci., Polym. Phys. Edn* 1976, **14**, 1731
16 Yang, X., Long, F., Shan, D. and Quian, R. *Polym. Commun.* 1991, **32**, 125
17 Heuvel, H. M. and Huisman, R. *J. Appl. Polym. Sci.* 1985, **30**, 3069
18 Lin, S. B. and Köenig, J. L. *J. Polym. Sci., Polym. Phys. Edn* 1983, **21**, 2365
19 Pastor, J. M., González, A. and de Saja, J. A. *J. Appl. Polym. Sci.* 1989, **38**, 2283
20 Stokr, J., Schneider, B., Doskocilová, D., Löry, J. and Sedlácek, P. *Polymer* 1982, **23**, 714
21 Lin, S. B. and Köenig, J. L. *J. Polym. Sci., Polym. Phys. Edn* 1983, **21**, 2067
22 Hutchison, I. J. and Ward, I. M. *Polymer* 1980, **21**, 55
23 Köenig, K. L. and Hannon, M. *J. Macromol. Sci. (Phys.)* 1967, **B1**, 119
24 Thompson, E. V. in 'Encyclopedia of Polymer Science and Engineering', Vol. 16, Wiley, New York, 1989, p. 711
25 Fakirov, S., Fisher, E. W., Hoffmann, R. and Schmidt, G. F. *Polymer* 1977, **18**, 1121
26 Groeninckx, G., Reynaers, H., Berghmans, H. and Smets, G. *J. Polym. Sci., Polym. Phys. Edn* 1980, **18**, 1311
27 Groeninckx, G. and Reynaers, H. *J. Polym. Sci., Polym. Phys. Edn* 1980, **18**, 1325
28 Lin, S. B. and Köenig, J. L. *J. Polym. Sci., Polym. Symp.* 1984, **71**, 121
29 Rao, M. V. S., Kumar, R. and Dweltz, N. E. *J. Appl. Polym. Sci.* 1986, **32**, 4439
30 Elenga, R., Seguela, R. and Rietsch, F. *Polymer* 1991, **32**, 1975
31 Blundell, D. J., Beckett, D. R. and Willcocks, P. H. *Polymer* 1981, **22**, 704
32 Köenig, J. L. 'Spectroscopy of Polymers', American Chemical Society, Washington, DC, 1992, p. 106
33 Rubin, I. I. in 'Encyclopedia of Polymer Science and Engineering', Vol. 8, Wiley, New York, 1987, p. 102
34 White, J. L. in 'Encyclopedia of Polymer Science and Engineering', Vol. 10, Wiley, New York, 1987, p. 634
35 Barres, O., Friedrich, C., Jasse, B. and Noël, C. *Makromol. Chem. Makromol. Symp.* 1991, **52**, 161
36 Aharoni, S. M., Sharma, R. K., Szobota, J. S. and Vernick, D. A. *J. Appl. Polym. Sci.* 1983, **28**, 2177
37 Murthy, N. S., Correale, S. T. and Minor, H. *J. Am. Chem. Soc.* 1991, **24**, 1185